Water Splitting Hot Paper

International Edition: DOI: 10.1002/anie.201502573
German Edition: DOI: 10.1002/ange.201502573

Heterostructure of Si and $CoSe_2$: A Promising Photocathode Based on a Non-noble Metal Catalyst for Photoelectrochemical Hydrogen Evolution**

Mrinmoyee Basu, Zhi-Wei Zhang, Chih-Jung Chen, Po-Tzu Chen, Kai-Chih Yang, Chong-Geng Ma, Chun Che Lin, Shu-Fen Hu, and Ru-Shi Liu**

Abstract: *Development of a solar water splitting device requires design of a low-cost, efficient, and non-noble metal compound as alternative to noble metals. For the first time, we showed that $CoSe_2$ can function as co-catalyst in photoelectrochemical hydrogen production. We designed a heterostructure of p-Si and marcasite-type $CoSe_2$ for solar-driven hydrogen production. $CoSe_2$ successively coupled with p-Si can act as a superior photocathode in the solar-driven water splitting reaction. Photocurrents up to 9 mA cm^{-2} were achieved at 0 V vs. reversible hydrogen electrode. Electrochemical impedance spectroscopy showed that the high photocurrents can be attributed to low charge transfer resistance between the Si and $CoSe_2$ interfaces and that between the $CoSe_2$ and electrolyte interfaces. Our results suggest that this $CoSe_2$ is a promising alternative co-catalyst for hydrogen evolution.*

In consideration of the upcoming energy crisis and current environmental issues, alternative and efficient green energy sources are urgently needed. In this respect, hydrogen is a very promising clean energy source, which can fulfill the energy demands. Photoelectrochemical (PEC) water splitting is a highly controlled approach to convert sunlight into clean and storable hydrogen and oxygen.[1] A large-scale effort has already been dedicated to find this alternative and also to fulfill the dream by generating higher photocurrent density.[2] However, the major problem in the PEC system is that it is very difficult for a single material to achieve all the requirements. Visible light-active materials suffer from photocorrosion, whereas wide-bandgap materials can be activated by UV light only. Higher photocurrents can be achieved by coupling two semiconductors with a type II band alignment. Nevertheless, the problem of sluggish hydrogen and oxygen evolution reaction rate decreases the efficiency of a material. Another approach to solve this problem is to decorate the semiconductor surface with a suitable co-catalyst, which further lowers the overpotential by increasing the kinetics of photoexcited electrons.[3]

The most fundamental aspects of PEC water splitting reactions are harvesting solar light, charge separation, and ready transportation of photogenerated carrier from the electrode surface to the electrolyte. For this purpose, p-type silicon with a bandgap of 1.1 eV, which is very economical and easy available, has been widely used as a photocathode in the PEC water splitting system.[4] However, the major drawback of silicon is the sluggish surface reaction and the chemical instability in different electrolyte solutions. External bias is required to avoid sluggish surface reactions of Si for spontaneous water splitting. Therefore, modification of the Si surface by a suitable co-catalyst and surface passivating material is highly significant for the practical application in PEC water splitting.[5] The noble metal Pt is known as the most efficient, stable co-catalyst for hydrogen evolution. However, the high cost and low availability of noble metals limit their wide-scale applicability. Thus, development of a low-cost material as an alternative to noble metals is extremely important. Recently, 3d transition-metal compounds have received much attention for their stability, low cost, and environmental friendliness. The 3d transition-metal compounds, such as alloys, sulfides, carbides, borides, selenides, and phosphides, are currently used as electrocatalysts for hydrogen and oxygen evolution reactions.[6] Among these compounds, the sulfides and selenides of Mo and W have been applied in the solar-driven hydrogen evolution reaction.[7] However, the PEC performance of non-noble metal compounds still needs improvement. Therefore, the development of suitable non-noble metal compounds with high performance is a great challenge.

Cobalt-based materials, such as cobalt–phosphate (Co-Pi), Co_3O_4, and other cobalt complexes, have been studied for hydrogen and oxygen evolution reactions.[8] Among the earth-abundant co-catalysts, $CoSe_2$ is recently studied as an electro-

[*] Dr. M. Basu, C. J. Chen, Dr. C. C. Lin, Prof. Dr. R. S. Liu
Department of Chemistry
National Taiwan University, Taipei 106 (Taiwan)
Prof. Dr. R. S. Liu
Department of Mechanical Engineering and Graduate Institute of Manufacturing Technology
National Taipei University of Technology, Taipei 106 (Taiwan)
E-mail: rsliu@ntu.edu.tw
Z. W. Zhang, P. T. Chen, K. C. Yang, Prof. Dr. S. F. Hu
Department of Physics
National Taiwan Normal University, Taipei 116 (Taiwan)
E-mail: sfhu.hu@ntnu.edu.tw
Prof. C.-G. Ma
College of Sciences
Chongqing University of Posts and Telecommunications
Chongqing 400065 (P.R. China)

[**] We are grateful for the financial support of the Ministry of Science, Technology of Taiwan (Contract No. MOST 103-2112M-003-009-MY3 and MOST 101-2113M-002-014-MY3) and Academia Sinica (Contract No. AS-103-TP-A06). C.-G. Ma would like to acknowledge financial support from the National Natural Science Foundation of China (Grant no. 11204393).

Supporting information for this article is available on the WWW under http://dx.doi.org/10.1002/anie.201502573.

catalyst for the oxygen and hydrogen evolution reaction with promising efficiencies.[9,10] Kong et al.[10] reported that $CoSe_2$ nanoparticles grafted on carbon fibers can achieve a photocurrent density of 100 mA cm^{-2} at an overpotential of about 0.18 V. Liu et al.[11] described ultrathin sheets of pyrite $CoSe_2$ for efficient oxygen evolution reaction with an overpotential of as low as 0.32 V at 10 mA cm^{-2} in pH 13. These first-row transition-metal dichalcogenides exist in two types of crystal structures: cubic (pyrite) and orthorhombic (marcasite).[10] We were motivated to apply marcasite $CoSe_2$ in PEC water splitting because our $CoSe_2$ nanorods on the glassy carbon electrode can achieve high electrocatalytic activity (24.6 mA cm^{-2} at 0.2 V) with improved onset potential in the hydrogen evolution reaction compared with the pyrite in a previous report.[10] The present study focuses on the efficient co-catalytic activity of $CoSe_2$ nanorod in PEC solar water splitting. This work is novel because for the first time, we studied the photo-electrochemical performance of marcasite $CoSe_2$.

In this study, we introduced an approach to synthesize marcasite $CoSe_2$ nanorods by following a simple hydrothermal route. After synthesis of $CoSe_2$ nanorods, it was decorated onto the surface of freshly etched Si microwires (MWs) by the spin-coating method. $CoSe_2$-decorated Si MWs ($Si/CoSe_2$) have been used as photocathode. A high current density of 9 mA cm^{-2} at 0 V vs. reversible hydrogen electrode (RHE) was achieved with excellent onset potential. With the increased catalyst loading on the Si MWs, the photocurrent density increased and the optimum photocurrent achieved was 14.12 mA cm^{-2} at −0.14 V vs. RHE (−0.40 V vs. Ag/AgCl). Electrochemical impedance spectroscopy was used to understand the superior efficiency of $CoSe_2$.

The $CoSe_2$ nanostructure was synthesized following an ethylenediaminetetraacetic acid ligand (EDTA)-assisted simple hydrothermal route and decorated on Si MWs by the spin-coating method. The Si MWs (resistivity: 1–15 Ω cm) were developed following our previously reported method.[12] The loading amount of $CoSe_2$ on Si MWs was varied and denoted as CT (C for $CoSe_2$; T = no of cycle in spin coating). To compare the performance of $Si/CoSe_2$, Si/Pt was also synthesized (for details, see the Supporting Information). Details of $CoSe_2$ synthesis and the decoration of Si MWs are discussed in the Experimental Section. The crystal structure of $CoSe_2$ is given in the Supporting Information, Figure S1. The crystallinity of the as-synthesized $CoSe_2$ deposited on Si MWs was determined from the Raman spectra shown in Figure 1 a. A sharp peak at 520 cm^{-1} was assigned to Si,[12] and another peak at 174 cm^{-1} was attributed to the stretching of Se−Se in $CoSe_2$.[13] The inset of Figure 1 a clearly shows the peak of Se−Se stretching. Notably, no additional peaks of impurities were observed.

The phase and crystallinity of $CoSe_2$ were determined by powder X-ray diffraction (PXRD). The typical PXRD pattern of $CoSe_2$ (Figure 1 b) clearly matches with JCPDS no. 89-2003. Rietveld refinement was carried out and the crystallographic parameters are shown in the Supporting Information, Table S1. $CoSe_2$ crystallizes under our present reaction condition in the orthorhombic crystal system with a marcasite-type structure. No other impurity peak is detected. EDTA played a major role in the synthesis of pure phase $CoSe_2$. In the absence of EDTA, $CoSe_2$ crystallized, with a strong peak of the Co_3O_4 impurity; the PXRD pattern can be seen in the Supporting Information, Figure S2. Under the present reaction conditions, Co^{II} forms a stable $[Co(EDTA)]^{2+}$ complex upon the reaction with EDTA, which restricts a faster reaction of Co^{II} with the hydroxide solution and further inhibits the formation of the Co_3O_4 impurity.

Scanning electron microscopy (SEM) images of bare Si MWs (length, 12 μm; width, 1 μm) is given in the Supporting Information, Figure S3, and the top view of the $Si/CoSe_2$ MWs (C20) is given in Figure 1 c (and the Supporting Information, Figure S4). $CoSe_2$ nanorods were synthesized using our proposed hydrothermal method. Moreover, the nanorods were decorated onto Si MWs by using our developed spin-coating method. The high-magnification SEM image shows that the average length of the $CoSe_2$ nanorod is about 300 nm and its width is about 50 nm. The SEM image (cross-sectional view) of $Si/CoSe_2$ is shown in Figure 1 d (and the Supporting Information, Figure S5), which is fully in accordance with the top-view SEM. Energy-dispersive X-ray spectroscopy (EDS) was used to determine the composition of the as synthesized material; from the spectra, we can see that the elements Si, Co, and Se are present (Supporting Information, Figure S6). Cross-sectional EDS mapping shows the distribution of Si along the route of MWs and the distribution of Co and Se on the top further confirms the presence of $CoSe_2$ on the top of Si MWs (Supporting Information, Figure S7). An XRD and an SEM image of Si/Pt is shown in the Supporting Information, Figure S8. Likewise, the morphology of the as-synthesized $CoSe_2$ was determined by transmission electron microscopy (TEM). A representative TEM image of $CoSe_2$ nanorods is shown in Figure 2 a. The nanorods are about 300 nm long and about 50 nm wide. The TEM images are in accordance with the observed SEM images of $CoSe_2$ nanorods. The inset of Figure 2 a shows a clearer view of $CoSe_2$ nanorods. An HRTEM image of the $CoSe_2$ nanorods is presented in Figure 2 b. The HRTEM image shows clear lattice fringes, which correspond to 0.26 nm and can be assigned to the spacing between the two (111) crystal planes. The XRD result also shows the highest intense peak for (111) plane.

The calculated band structure diagrams for $CoSe_2$ are shown in the Supporting Information, Figure S9. The position of the Fermi energy levels (E_F) in this compound indicates its half-metallic nature. The calculated bandgap for beta electrons in $CoSe_2$ has an indirect character (SM→DT) and is equal to 1.7837 eV. The partial and total densities of states (PDOS/DOS) of $CoSe_2$ have been calculated; the diagrams are given in Figure 3. Very strong hybridization between the Co 3d and Se 4p states is easily seen. Moreover, a bandgap exists between the t_{2g} and e_g states for the beta electrons; that is, their half-metallic character is further confirmed by the PDOS/DOS analyses.

By utilizing the advantages of semi-metallic behavior of $CoSe_2$ nanorods, $Si/CoSe_2$ heterostructure can remarkably enhance the efficiency of the PEC water splitting system. The photoresponse of bare Si MWs was initially measured by etching the native oxide layer for 30 s in 10 % aqueous

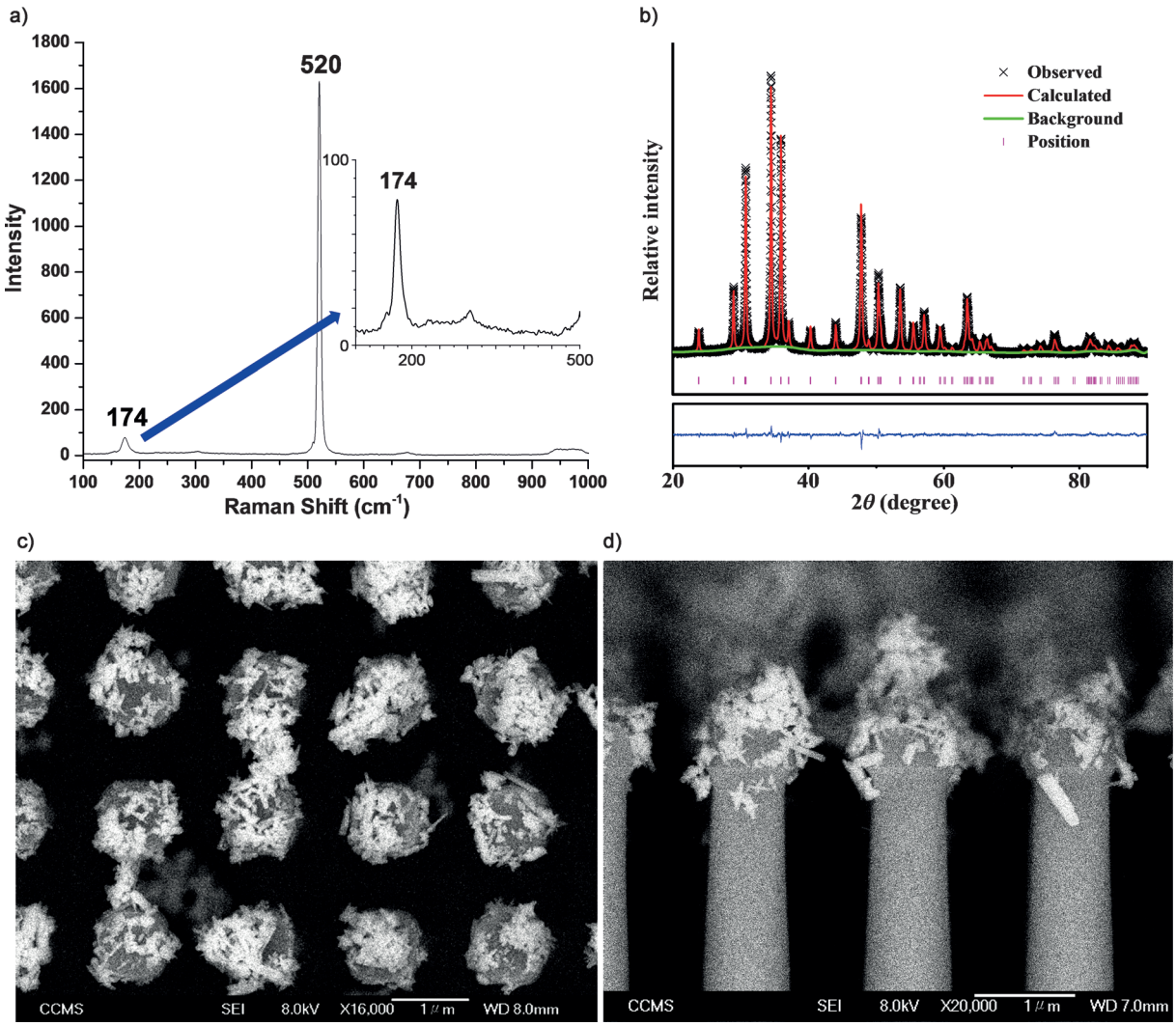

Figure 1. a) Raman spectra and b) PXRD pattern of $CoSe_2$. SEM images of $CoSe_2$ nanorods decorated on Si MWs (C20), c) top and d) cross-sectional views.

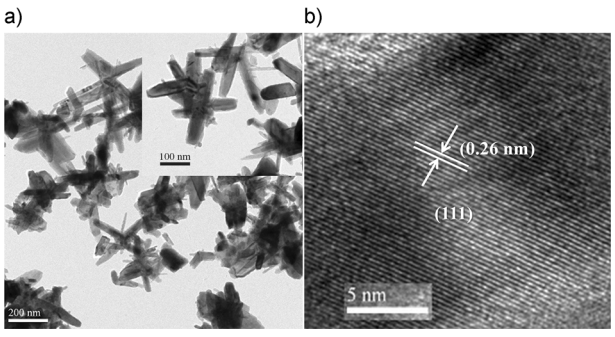

Figure 2. a) TEM and b) HRTEM images of $CoSe_2$ nanorods.

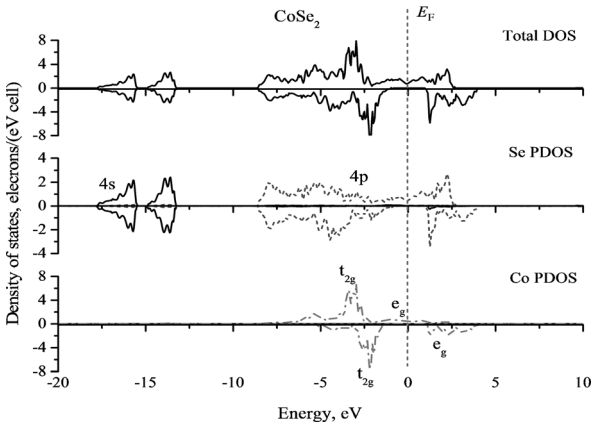

Figure 3. Calculated PDOS/DOS diagrams for $CoSe_2$. The vertical dashed line denotes the Fermi level position. —— s states, ----- p states, –•–• d states.

hydrofluoric acid (HF) solution. Given an applied potential of −0.94 V vs. RHE (−1.2 V vs. Ag/AgCl), Si MWs can achieve an 8 mA cm^{-2} photocurrent with an onset potential of −0.49 V vs. RHE (−0.75 V vs. Ag/AgCl; Supporting Information, Figure S10). The PEC water splitting of Si/$CoSe_2$ is performed within the applied potential range of 0.46 V to −0.14 V vs. RHE. Figure 4a shows that a very small amount of $CoSe_2$ (C5) can successively increase the photocurrent density of approximately 10.5 mA cm^{-2} at a potential of

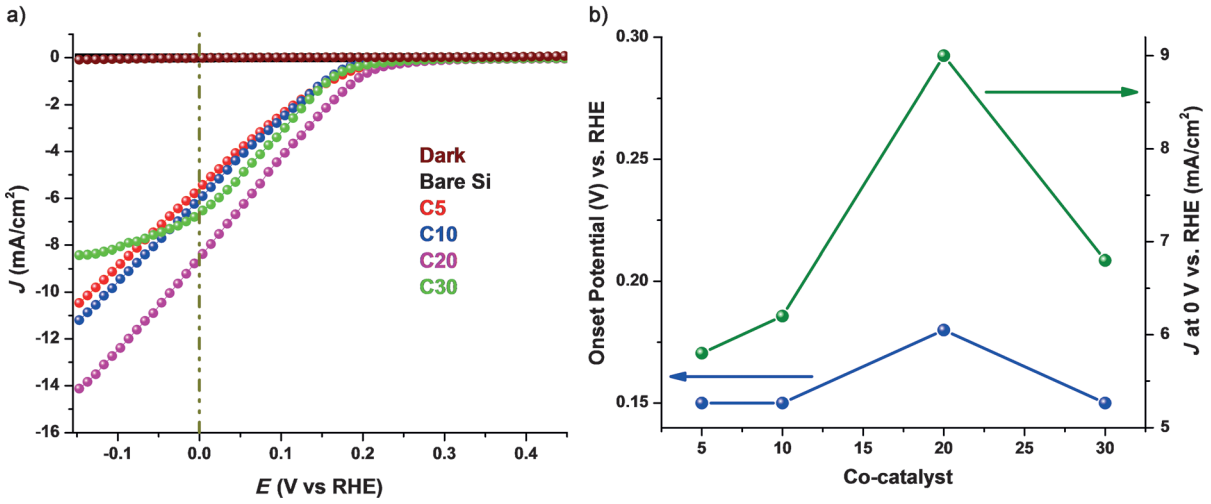

Figure 4. a) Linear-sweep voltammograms of bare Si and Si/$CoSe_2$ (C*T*, *T* = 5, 10, 20, 30). b) Current density at 0 V vs. RHE and onset potentials with respect to $CoSe_2$ loading.

−0.14 V vs. RHE with an onset potential of 0.15 V vs. RHE. At 0 V vs. RHE, a photocurrent density of 5.8 mA cm^{-2} is achieved. Compared with bare Si, a successive increase in the photocurrent density and a positive shift in the onset potential are obtained. Si/$CoSe_2$ shows a very negligible dark current. The photocurrent density is successively increased with increasing amount of decorated $CoSe_2$ nanorods. In the present potential window, bare Si MWs do not show any photoresponse. A successive increase in the amount of $CoSe_2$ nanorods (C20) shifts the onset potential to 0.18 V vs. RHE, with improved current density. The optimum current density of 14.12 mA cm^{-2} was observed with an applied potential of −0.14 V vs. RHE. At 0 V potential vs. RHE, the photocurrent density was enhanced to 9 mA cm^{-2}. The semi-metallic nature of $CoSe_2$ leads to enhanced transportation of photo-excited electrons from the semiconductor surface to the electrolyte. With more increased decoration of $CoSe_2$ nanorods on the Si MW surface, the photocurrent density strongly decreased to 8.40 mA cm^{-2} at −0.14 V and 6.80 mA cm^{-2} at 0 V vs. RHE. The certain drop in photocurrent density may be attributed to two reasons. First, accumulation of more $CoSe_2$ at the top of Si MWs may inhibit the light absorption, which further decreases the photocurrent density. Second, increased amounts of the co-catalyst can act as charge recombination centers, which decreases the charge transportation and further decreases the PEC performance. Therefore, from the observed photocurrent density, a typical volcano-type trend was observed between the loading amount of $CoSe_2$ nanorods on Si MWs and the photocurrent density, which is in accordance with previous reports.[6a] Both the onset potential and the photocurrent density at 0 V vs. RHE follow the same volcano-type trend (Figure 4b) present in the optimal co-catalyst loading of C20. The loading of $CoSe_2$ in C20 was evaluated with the help of the ICP (inductively coupled plasma)-mass, which is about 0.36 mg cm^{-2}, and the calibration curve is shown in the Supporting Information, Figure S11. Consecutive scans of Si/$CoSe_2$ (C20) show a negligible decrease in the photocurrent density upon photo-irradiation (Supporting Information, Figure S12). Photocurrent density of C20 is compared with our synthesized Si/Pt MWs, which shows that the performance of C20 is comparable with Si/Pt (Supporting Information, Figure S13).

In our study, the most used Si/$CoSe_2$ photoelectrode is the C20 electrode, which can achieve optimum photocurrent density with high consistency (Supporting Information, Figure S14). The transient current of the Si MWs and Si/$CoSe_2$ (C20) was measured at 0.08 V vs. RHE under pulsed illumination (Supporting Information, Figure S15). Under pulsed illumination, the Si/$CoSe_2$ (C20) electrode demonstrated a transient switch-on characteristic, but bare Si does not show any photoresponse in the applied potential window. The gas evolution rates of hydrogen and oxygen of Si/$CoSe_2$ (C20) were 1.77 and 0.83 μmol min^{-1}, respectively. The Faradic efficiency of hydrogen and oxygen evolution was 61% and 54%, respectively, under the applied potential −0.10 V vs. RHE in 20 min (Supporting Information, Figure S16). To understand the stability of the photoelectrode, the electrochemical stability of the as-synthesized $CoSe_2$ was evaluated. The electrochemical performance of $CoSe_2$ was checked by a three electrode system in 0.5 M H_2SO_4. After 50 consecutive cycles, the changes in the current density and the onset potential are very negligible (Supporting Information, Figure S17). This result implies that orthorhombic $CoSe_2$ is efficient and stable under the given electrochemical conditions.

UV/Vis spectroscopy was used to compare the drop in the photocurrent density of C30 compared to C20. We measured the optical properties of C5, C20, C30, and bare Si, as shown in Figure 5b. Although the tops of the Si MWs were decorated by $CoSe_2$, the absorption of visible light by Si MWs was not inhibited. C20 and C30 have nearly the same light absorption profiles. Therefore, a excess amount of co-catalyst does not restrict the optical absorption of Si. Furthermore, the drop in the photocurrent density from C20 to C30 cannot be attributed to the decreased optical absorption.

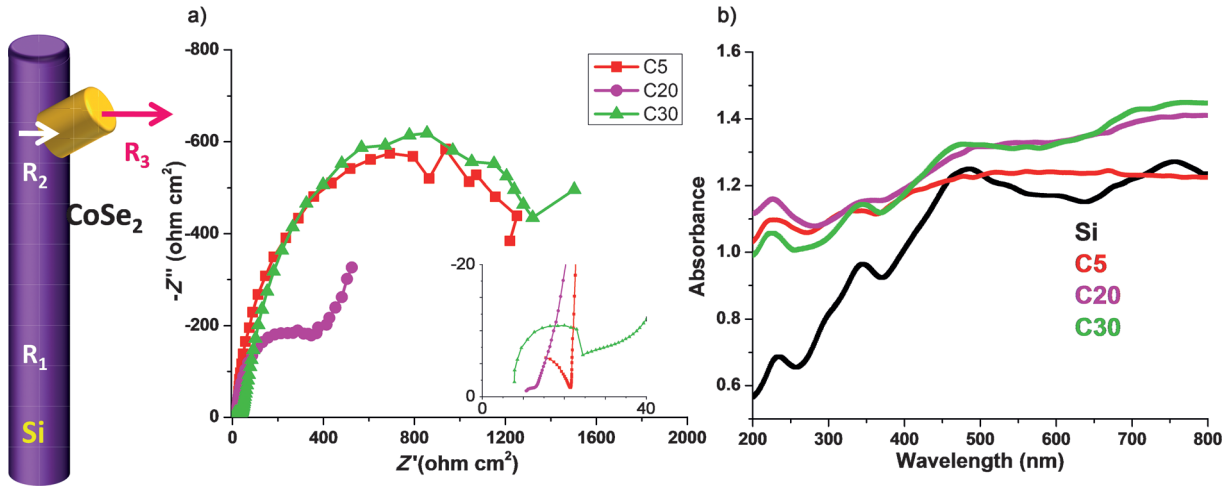

Figure 5. a) Nyquist impedance plots of CT ($T = 5$, 20, 30) measured under light irradiation. b) UV/Vis absorption spectra of Si and Si/$CoSe_2$ (CT, $T = 5$, 20, 30).

To attain a clear understanding of the PEC performance, an impedance study was carried out to determine the feasibility of charge transfer on different photocathode surfaces. The impedance was measured under illumination at 0.15 V vs. RHE (−0.1 V vs. Ag/AgCl). The Nyquist plot shows that all the photocathodes have two distinguished semicircles (Figure 5a). The evaluated data can be fitted with an equivalent circuit consisting of constant phase elements (CPE) for the semiconductor Si (CPE_{Si}) and the co-catalyst $CoSe_2$ (CPE_{CoSe_2}) as well as Wo, which is called the Warburg constant. Two kinds of charge transfer resistance R_2 ($R_{ct,Si}$) and R_3 ($R_{ct,CoSe_2}$) are present. $R_{ct,Si}$ signifies the coupling between the semiconductor Si MWs and the co-catalyst $CoSe_2$, whereas $R_{ct,CoSe_2}$ refers to the charge transfer resistance between $CoSe_2$ and electrolytes, which further implies the co-catalytic activity of $CoSe_2$. Impedance curve of C5 and C30 has been fitted by equivalent circuit "A" ignoring the very small diffusion part of C30 and C20 by "B" (Supporting Information, Figure S18). The resistance values are summarized in the Supporting Information, Table S3. The charge-transfer resistance from Si to $CoSe_2$ for C5 (6.0 $\Omega\,cm^2$) and C20 (5.8 $\Omega\,cm^2$) are almost equal. However, $R_{ct,Si}$ for the C30 electrode was increased to 18.9 $\Omega\,cm^2$. The increased value of $R_{ct,Si}$ for the C30 focus hindered charge caused by the increased amount of co-catalyst on Si MWs. The charge transfer resistance from $CoSe_2$ to electrolyte ($R_{ct,CoSe_2}$) of the C20 electrode is significantly lower than that of C5 and C30. The $R_{ct,CoSe_2}$ value of C20 (270 $\Omega\,cm^2$) was strongly decreased relative to that of C5 (1300 $\Omega\,cm^2$), which implies the increased charge transfer from Si/$CoSe_2$ to the electrolyte with the increased amount of semi-metallic $CoSe_2$ on Si MWs. $R_{ct,CoSe_2}$ value for C30 significantly increased from 270 $\Omega\,cm^2$ to 1450 $\Omega\,cm^2$, with very minimal ion diffusion.

In case of C20, facile charge transfer takes place along with diffusion of ions, which promotes for superior activity. Distribution of $CoSe_2$ nanorods especially on the top of Si MWs infer about the higher quality interface of Si and $CoSe_2$. From the observed results, we can predict that the increased co-catalyst accumulation on the semiconductor surface functions as charge recombination centers with low quality interface which further restricts the charge transfer, thereby increasing the resistance value. From the PEC result also it is evident that C30 can reach to saturation current density but not for C5 and C20. The impedance results are consistent with our as-observed PEC results.

In summary, we demonstrated for the first time that semi-metallic $CoSe_2$ is an active co-catalyst for hydrogen evolution in PEC water splitting reaction. We synthesized orthorhombic $CoSe_2$ nanorods using a simple hydrothermal technique, and then decorated the nanorods on Si MWs. The semi-metallic nature of orthorhombic $CoSe_2$ is revealed. This property of $CoSe_2$ promotes faster electron transfer from Si to the $CoSe_2$ surface and finally to the electrolyte. Consequently, the synthesized heterostructure of Si/$CoSe_2$ had a photocurrent density of as high as 14.12 mA cm^{-2}, with strong shift of onset potential 0.18 V vs. RHE. The excellent performance of Si/$CoSe_2$ indicates that this material a promising alternative for noble metal-based photocathodes.

Experimental Section

The $CoSe_2$ nanostructure was synthesized by a simple hydrothermal route following a previously reported route with some modifications.[14] First, two solutions were prepared. Solution A was prepared by mixing 0.5 M EDTA ligand in an aqueous solution (5 mL) and 2 mmol cobalt(II) chloride hexahydrate (5 mL). Solution B was prepared by dissolving Se powder (4 mmol) in 3.3 M NaOH (30 mL). Solutions A and B were separately sonicated for 15 min before both solutions were thoroughly mixed. Finally, a 40 mL aliquot of the reaction solution was transferred to a 100 mL Teflon-lined autoclave. The hydrothermal reaction was performed at 180 °C for 18 h. After the reaction was completed, the autoclave was allowed to cool naturally. The black precipitate was washed thoroughly with water and acetone. The product was dried at 50 °C for 30 min and stored for further characterization. The role of EDTA in the reaction has been previously examined and discussed.

The as-synthesized $CoSe_2$ nanorods were used to decorate the Si MW surface. Si MW was synthesized according to our previously reported method. $CoSe_2$ was dispersed in ethanol dispersion at a concentration of 0.3 mg mL^{-1}. The $CoSe_2$ was dispersed for 12 h by

ultrasonication. The $CoSe_2$ dispersion was then spin coated on to Si MWs. At the time of spin coating, 1 mL of the $CoSe_2$ solution was slowly dropped onto Si MW wafers for 5 min at 500 rpm. Subsequently, the Si MW was dried at 60 °C for 10 min. These two steps are counted as one cycle. In this manner, we prepared our $Si/CoSe_2$ electrodes, which were denoted as C*T* (where *T* is the number of cycles for spin coating). Pt nanoparticles are also synthesized on Si MW surface and the detail is given in the Supporting Information.

Keywords: cobalt selenide · hydrogen evolution · nanorods · semi-metals · water splitting

How to cite: *Angew. Chem. Int. Ed.* **2015**, *54*, 6211–6216
Angew. Chem. **2015**, *127*, 6309–6314

[1] A. Fujishima, K. Honda, *Nature* **1972**, *238*, 37.
[2] a) Z. Huang, Z. Chen, Z. Chen, C. Lv, H. Meng, C. Zhang, *ACS Nano* **2014**, *8*, 8121; b) H. M. Chen, C. K. Chen, R. S. Liu, L. Zhang, J. Zhang, D. P. Wilkinson, *Chem. Soc. Rev.* **2012**, *41*, 5654.
[3] S. C. Riha, B. M. Klahr, E. C. Tyo, S. Seifert, S. Vajda, M. J. Pellin, T. W. Hamann, A. B. F. Martinson, *ACS Nano* **2013**, *7*, 2396.
[4] X. Li, Y. Xiao, K. Zhou, J. Wang, S. L. Schweizer, A. Sprafke, J.-H. Lee, R. B. Wehrspohn, *Phys. Chem. Chem. Phys.* **2015**, *17*, 800.
[5] a) J. R. McKone, E. L. Warren, M. J. Bierman, S. W. Boettcher, B. S. Brunschwig, N. S. Lewis, H. B. Gray, *Energy Environ. Sci.* **2011**, *4*, 3573; b) M. J. Kenney, M. Gong, Y. Li, J. Z. Wu, J. Feng, M. Lanza, H. Dai, *Science* **2013**, *342*, 836; c) S. Hu, M. R. Shaner, J. A. Beardslee, M. Lichterman, B. S. Brunschwig, N. S. Lewis, *Science* **2014**, *344*, 1005.
[6] a) J. Ran, J. Zhang, J. Yu, M. Jaroniec, S. Z. Qiao, *Chem. Soc. Rev.* **2014**, *43*, 7787; b) Y.-H. Chang, R. D. Nikam, C.-Te. Lin, J.-K. Huang, C.-C. Tseng, C.-L. Hsu, C.-C. Cheng, C.-Y. Su, L.-J. Li, D. H. C. Chua, *ACS Appl. Mater. Interfaces* **2014**, *6*, 17679; c) H. Vrubel, X. Hu, *Angew. Chem. Int. Ed.* **2012**, *51*, 12703; *Angew. Chem.* **2012**, *124*, 12875; d) E. J. Popczun, C. G. Read, C. W. Roske, N. S. Lewis, R. E. Schaak, *Angew. Chem. Int. Ed.* **2014**, *53*, 5427; *Angew. Chem.* **2014**, *126*, 5531.
[7] a) Z. Huang, C. Wang, Z. Chen, H. Meng, C. Lv, Z. Chen, R. Han, C. Zhang, *ACS Appl. Mater. Interfaces* **2014**, *6*, 10408; b) Y. Li, H. Wang, L. Xie, Y. Liang, G. Hong, H. Dai, *J. Am. Chem. Soc.* **2011**, *133*, 7296; c) Q. Ding, F. Meng, C. R. English, M. Caban-Acevedo, M. J. Shearer, D. Liang, A. S. Daniel, R. J. Hamers, S. Jin, *J. Am. Chem. Soc.* **2014**, *136*, 8504.
[8] a) X. Chen, H. Ren, W. Peng, H. Zhang, J. Lu, L. Zhuang, *J. Phys. Chem. C* **2014**, *118*, 20791; b) J. J. H. Pijpersa, M. T. Winkler, Y. Surendranath, T. Buonassisi, D. G. Nocera, *Proc. Natl. Acad. Sci. USA* **2011**, *108*, 10056.
[9] M.-R. Gao, X. Cao, Q. Gao, Y.-F. Xu, Y.-R. Zheng, J. Jiang, S.-H. Yu, *ACS Nano* **2014**, *8*, 3970.
[10] D. Kong, H. Wang, Z. Lu, Y. Cui, *J. Am. Chem. Soc.* **2014**, *136*, 4897.
[11] Y. Liu, H. Cheng, M. Lyu, S. Fan, Q. Liu, W. Zhang, Y. Zhi, C. Wang, C. Xiao, S. Wei, B. Ye, Y. Xie, *J. Am. Chem. Soc.* **2014**, *136*, 15670.
[12] C. J. Chen, M.-G. Chen, C. K. Chen, P. C. Wu, P.-T. Chen, M. Basu, S.-F. Hu, D. P. Tsai, R.-S. Liu, *Chem. Commun.* **2015**, *51*, 549.
[13] H. Zhang, L. Lei, X. Zhang, *RSC Adv.* **2014**, *4*, 54344.
[14] W. Zhang, Z. Yang, J. Liu, Z. Hui, W. Yu, Y. Qian, G. Zhou, L. Yang, *Mater. Res. Bull.* **2000**, *35*, 2403.

Received: March 19, 2015
Published online: April 29, 2015

